Fluid Dynamics Research

The Japan Society of Fluid Mechanics

PAPER

On angled bounce-off impact of a drop impinging on a flowing soap film

IOP Publishing | The Japan Society of Fluid Mechanics Fluid *Dynamics* Research

Fluid Dyn. Res. **49** (2017) 065509 (19pp) https://doi.org/10.1088/1873-7005/aa9280

On angled bounce-off impact of a drop impinging on a flowing soap film

Saikat Basu[1,4], **Ali Yawar**[1,5], **Andres Concha**[2,3] and **M M Bandi**[1]

[1] Collective Interactions Unit, Okinawa Institute of Science and Technology Graduate University, Onna-son, Okinawa 904-0495, Japan
[2] Condensed Matter i-Lab, Diagonal las Torres 2640, Building D, Peñalolen, Santiago, Chile
[3] School of Engineering and Sciences, Universidad Adolfo Ibañez, Diagonal las Torres 2640, Peñalolen, Santiago 7941169, Chile

E-mail: saikat_basu@med.unc.edu

Received 16 May 2017, revised 4 October 2017
Accepted for publication 6 October 2017
Published 15 November 2017

Communicated by Professor Anne Juel

Abstract

Small drops impinging obliquely on thin flowing soap films frequently demonstrate the rare emergence of bulk elastic effects working in-tandem with the more commonplace hydrodynamic interactions. Three collision regimes are observable: (a) drop piercing through the film, (b) it coalescing with the flow, and (c) it bouncing off the film surface. During impact, the drop deforms along with a bulk elastic deformation of the film. For impacts that are close-to-tangential, the bounce-off regime predominates. We outline a reduced order analytical framework assuming a deformable drop and a deformable three-dimensional film, and the idealization invokes a phase-based parametric study. Angular inclination of the film and the ratio of post and pre-impact drop sizes entail the phase parameters. We also perform experiments with vertically descending droplets (constituted from deionized water) impacting against an inclined soap film, flowing under constant pressure head. Model-predicted phase domain for bounce-off compares well to our experimental findings. Additionally, the experiments exhibit momentum transfer to the film in the form of shed vortex dipoles, along with propagation of free surface waves. On consulting prior published work, we note that for locomotion of water-walking insects using an impulsive action, the momentum distribution to the shed vortices and waves are both significant, taking

[4] Currently at the Computing and Clinical Research Lab (Biomathematical Modeling), Department of Otolaryngology, University of North Carolina at Chapel Hill – School of Medicine, Chapel Hill, NC 27599, United States of America.
[5] Currently at the Biomechanics and Control Lab, Department of Mechanical Engineering and Materials Science, Yale University, New Haven, CT 06520, United States of America.

up respectively $2/3$ and $1/3$ of the imparted streamwise momentum. Considering the visually similar impulse actions, this theory, despite its assumption of a quiescent liquid bath of infinite depth, is applied to the drop bounce-off experiments, and the resultant shed vortex dipole momenta are compared to the momenta of the coherent vortex structures computed from particle imaging velocimetry data. The magnitudes reveal identical order (10^{-7} N s), suggesting that notwithstanding the disparities, the bounce-off regime may be tapped as a toy analog for impulse-based interfacial biolocomotion.

Keywords: drop impact, soap film, interfacial flow, bouncing drops

(Some figures may appear in colour only in the online journal)

1. Introduction

Interactions where the bulk elastic properties of a fluidic system as well as the hydrodynamic effects assume comparable significance are a rarity. Consideration of elastic effects in problems of fluid mechanics is, in most situations, restricted towards accounting for the surface stretching that leads to interfacial tension. For a soap film, owing to the minuscule thickness, it is often a robust idealization to assume that its dynamic behavior is similar to that of a stretched two-dimensional membrane, thereby implying that considering bulk elasticity would be superfluous. This assumption can be traced back to various articles in literature on soap film dynamics and interactions. E.g. Bandi *et al* (2013) have explored the oscillatory instability of pendula embedded in a flowing soap film, Salkin *et al* (2016) have analyzed the impact dynamics of a gas jet on a vertically flowing soap film, while an expository study on soap film hydrodynamics came from Couder *et al* (1989). Vortex wakes shed by bluff bodies in a flowing soap film also serve as experimental reference points for point vortex theories owing to the approximate two-dimensionality of the films, see e.g. Basu and Stremler (2017), Stremler *et al* (2011), Stremler and Basu (2014), Basu (2014). However, to gain a physical understanding of a more complicated soap film interaction, the current work proposes a model system which demonstrates in-tandem effects of both hydrodynamics and the bulk elasticity. It involves very small drops (with diameters approximating 1.2–1.4 mm) impinging into a flowing soap film, wherein the nature of post-impact dynamics is affected by the three-dimensionality of the film material. During the impact, the drop shoots into the film surface and deforms it, thereby generating a bulk restitutive reaction. The drop also deforms and spreads out on impact. Salient hydrodynamic effects like shed vortices, owing to the shear layers generated from the relative motion between the gravity-driven drop and the film flow, emerge during the interaction. Such interactions can be broadly classified into: (a) the drop hits the film surface, moves downstream for a finite time, and then disconnects and bounces off the surface (designated as the *bounce-off* regime), (b) the drop hits the film surface and moves downstream with the background stream (*coalescence* regime), and (c) the kinetic energy of the descending drop is high enough to make it tunnel down through the film (*piercing* regime). See figure 1 for a schematic representation of these three major regimes of drop impact.

It is important to note that a larger drop size significantly complicates the dynamics leading to a 'pinch-off' regime, wherein a part of the drop connects with the flow and is sheared away while the rest of the drop mass persists to track an inertial trajectory off the film surface. Chen *et al* (2006) have studied the influence of viscosity on such pinch-off effects. Such interactions, often also referred to as 'partial colescence' (see e.g. Thoroddsen and

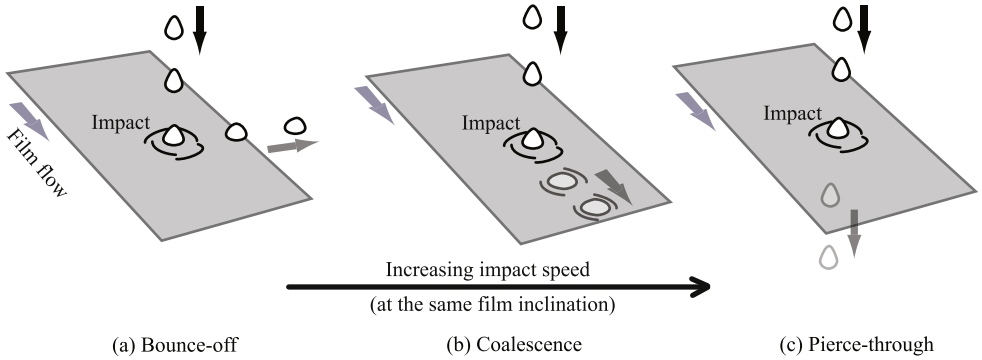

Figure 1. Artistic representations of the three broadly observable collision regimes when drops impinge on a soap film: (a) bounce-off, (b) coalescence, and (a) pierce-through. In each panel, the vertical dark arrow represents the drop's pre-impact descent direction, the slanted arrow beside the soap film (colored light gray) shows the film's direction of flow, and the gray slanted arrow adjacent to the post-impact drop indicates the corresponding drop motion.

Takehara (2000), Honey and Kavehpour (2006), Gilet *et al* (2007)), are however beyond this work's purview.

We have performed a series of experiments where the drop hits the film surface at a shallow angle ($<10°$), which is the angle subtended between the film 'plane'[6] and the vertically downward pre-impact trajectory of the incident drop. The angle has been marked as θ in figure 2 – an artistic rendering of the experimental setup. Bounce-off regime predominates for such close-to-tangential impacts. A quasi two-dimensional projection of the resultant impact is remarkably similar in several aspects to the impulsive interaction observed in water strider locomotion at air–water interfaces (albeit, with the depth of the liquid bath being considered infinite in the scale of the problem), as studied for example by Hu *et al* (2003). For higher angles of impact, the pierce-through regime gains precedence, as pointed out in the work of Kim and Wu (2010). Amongst results related to this regime, Kirstetter *et al* (2012) have looked at passage of liquid jets through a film without rupturing it. Le Goff *et al* (2008) have investigated the motion of impacting projectiles (consisting of beads smaller than the capillary length) piercing through inclined films.

The components of this article can be schematized into: (a) experimental visualization of drops impacting the film at shallow angles, (b) developing a reduced order mathematical model to identify a distinct phase domain for the observed bounce-off regime, with the phase parameters comprising the angular inclination of the film and the on-impact deformation features of the drop, (c) comparing the model predictions with experimental observations, thereby gaining an insight into the efficacy of the reduced order idealizations, and (d) identifying the relevance of the impulsive nature and momentum transfer observed in this bounce-off regime with reference to the interfacial locomotion of animals living at the water–air interface[7].

For additional study on similar bouncing interactions, see Courbin *et al* (2006)'s work related to bouncing of solid beads on a stationary elastic membrane. Jayaratne and Mason (1964) and

[6] Note that the so-called film 'plane' is not a truly planar surface. The film has undulating ripples and typically may have a subtle sagging. When we mention the angle subtended by the film's plane with the vertical, it is essentially the angle between the wire, holding the film, and the vertical.

[7] Note that Gerridae, some beetles, are however not classified as 'aquatic' (Cheng 1985), despite portraying such air–water interfacial locomotion.

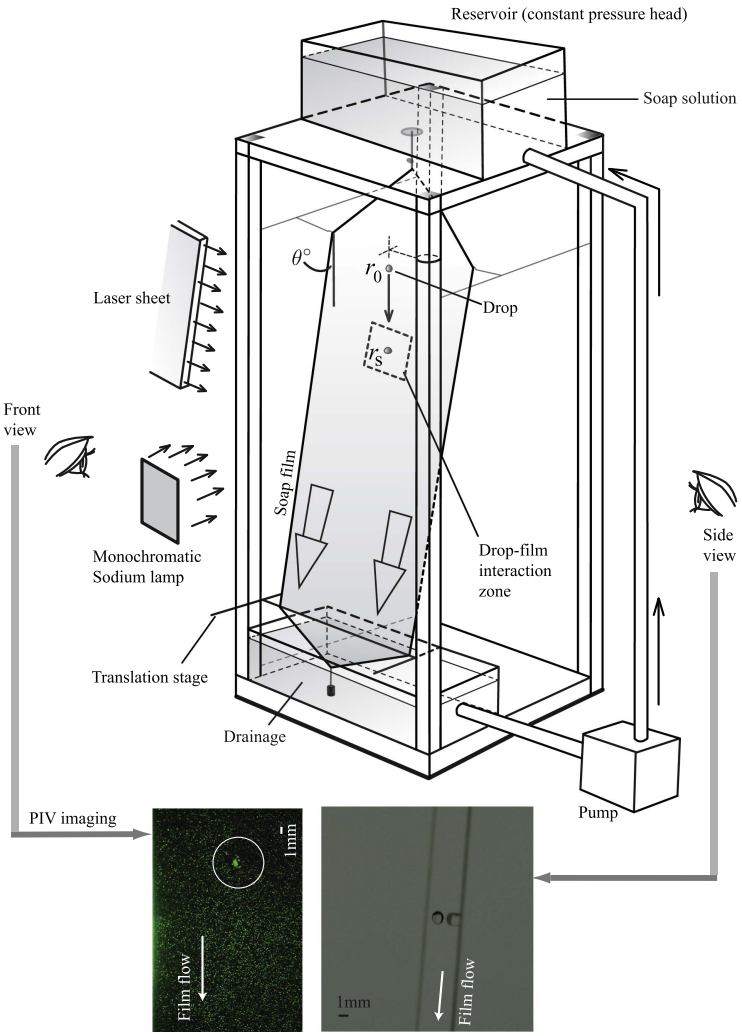

Figure 2. An artistic schematic of the experimental setup. The soap water flows steadily through a wired network under a constant pressure head maintained at the overhead reservoir through re-circulatory pumping. Width of the film is 5 cm, and the length is approximately 194 cm. Soap solution concentration is 2.5% by volume in deionized water. θ represents the angle subtended by the soap film with the vertical, r_0 is the pre-impact radius of the drop (assuming it to be spherical), r_s is the spread radius of the drop as it impinges into the soap film. In other words, r_s is the radius of the circular peripheral intersection of the impinged drop with the film plane. See sections 2.1, 3.1.1, 3.1.2, 3.1.3 for details about the soap solution and its rheology. Two cameras were used to record the interaction. Side view: along the plane of the film, which was lit by diffused white light, and front view: perpendicular to the plane of the film lit by monochromatic sodium light with wavelength $\lambda = 532$ nm. For flow field measurements through the particle imaging velocimentry (PIV) technique, an optical setup produced a laser sheet passing through the film and recorded by the front camera. Inset snapshots at the bottom representatively depict the corresponding camera visualizations. Note that the setup illustration is *not-to-scale*.

Pan and Law (2007) have explored the criteria for bouncing versus coalescence for droplets striking the free surface of a fluid bath, with the liquid layer backed off by a solid surface. Chaotic bouncing of a droplet on a soap film has been investigated by Gilet and Bush (2009a), along with a more intensive treatment in Gilet and Bush (2009b). More recently, Gilet and Bush (2012) have looked at droplets bouncing on a wet, inclined rigid surface with a thin coating of highly viscous fluid. Okumura *et al* (2003) have studied bounce-off motion of liquid balls on a rigid surface using a spring-mass idealization, with the ball undergoing small deformations. Mass-spring damper models have also been employed by Terwagne *et al* (2013) to explore vertically bouncing drops on a low viscous oil bath that is vibrated, assuming that the drop deforms while the deformation of the bath is negligible. Gopinath and Koch (2001), Courbin and Stone (2006), and Gilet and Bush (2009b) have provided Weber number (*We*) based characterization for bounce-off dynamics. With the surface tension of the film as σ, then for the pre-impact drop speed v_i, drop radius r_0, and drop fluid density $\tilde{\rho}$, the dimensionless Weber number computes to $We = \tilde{\rho} v_i^2 r_0 / \sigma$. Evidently, *We* is proportional to the initial kinetic energy of the falling drop, and a higher *We* leads to pierce-through without breaking the film, while a lower *We* corresponds to the bounce-off regime. These energy-based investigations (Courbin and Stone (2006), Gilet and Bush (2009b)), which were for horizontal stationary films impinged upon by vertically descending droplets, presented phase domain analysis on a plane consisting of *We* and the size ratio of the incident drop and the stretched-out circular soap film. In our work, we identify a different set of phase parametric criteria (angular orientation of the inclined soap film and the spreading characteristics of the drop on impact) for the bounce-off motion and justify the regime's phase location through a broad set of experimental data.

Preliminary reports on this work have been presented at the annual meeting of the APS Division of Fluid Dynamics in Boston, MA, November 2015 (Basu *et al* (2015), Yawar *et al* (2015)).

2. Experimental parameters and observations

2.1. Soap film setup

Soap films used in our study can be described, in simple terms, as sheets of water with a typical thickness of 1–10 μm ('thick films'; see Couder *et al* (1989), Gharib and Derango (1989)), and covered with surfactant (soap molecules) on the two sides at the water–air interfaces. The surfactant imparts elasticity to the film, thereby making the system more resistant to rupturing. Beyond a surfactant concentration threshold, along with coating the film surfaces, the dissolved surfactant molecules cluster as micelles inside the interstitial fluid. While thick films are governed by hydrodynamic principles, effects like van der Waals forces and double layer repulsion (Lyklema and Mysels 1965) can gain precendence with thinning. Amongst the more recent contributions, the study by Rutgers *et al* (2001) offers a comprehensive discussion on the use of flowing soap films as an experimental device.

The soap film setup (see figure 2) consists of two parallel nylon fishing lines (of thickness 0.3 mm and length ~2.0 m, each), hanging taut with a spanwise separation of 5 cm. On the top, the lines are tied together to a plastic overhead reservoir containing soap solution (Dawn™ dish-washing soap dissolved in deionized water with a concentration of 2.5% by volume), through a flow control valve. A re-circulatory pumping system, comprising a micro pump (Micropump®, GJ Series) with an AC drive (Micropump®, DP-415A.A), preserves the pressure head at the reservoir. The latter has a level sensitive drain, and is constantly refilled (via the pumping network) with soap solution that drains to the bottom of the fishing lines, where a hanging mass keeps them taut. Four nylon guide strings wrap around the cords to keep them separated. By controlling the

flow rate and maintaining a constant pressure head, we ensure a steady flowing soap film. Interferometry results suggest that the film thickness is roughly in the order of microns. The averaged pre-impact drop diameter is approximately 1.3 ± 0.1 mm. The observational errors can be traced to the annular thickness of the drop 'halo', owing to the imaged bright peripheries of the drop surface. The film length is 194 cm streamwise and the cross-stream film width is 5 cm, the latter being controlled by the transverse stream separation of the wires. As discussed later (see section 3.1.1), we work with a sufficiently large width of a film so that the surface waves generated upon impact do not affect the subsequent drop dynamics. The experimental rig is constructed using commercially available 80/20 pieces. We use fresh soap solution, and the plumbing is flushed with deionized water before every trial to keep the system free of debris (like rust particles).

By controlling the horizontal displacement of the bottom end with respect to the top using a translation stage, the film is inclined at 8 different angles (ranging from 0.86° to 6.85°) to the vertical. Above these angles, the film starts to sag. As mentioned already, for higher angles of impact, the puncture of the film leading to the drop tunneling through it becomes a more common occurrence. Figure 3 demonstrates a representative bounce-off case, imaged from the side with the line of sight being almost in-plane with the film orientation.

Special note should be made of the choice of a flowing soap film, instead of a static one. The thickness of a stationary soap film will vary (it will be draining), therefore each measurement will have an extra unknown factor. However, in an inclined flowing film under the same conditions, the film thickness is well-controlled. It may still not be a constant as there is a surface profile, but such thickness variations are reproducible (Kim and Wu 2010). Also, a flowing film allows for a direct comparison of the flow speed and the surface wave speed, the latter being generated from the impact of the drop on the film.

2.2. Drop generation

A Terumo^{TM} (Terumo Corporation, Tokyo, Japan) 33G syringe needle, connected to a syringe pump (Harvard Apparatus^{TM} – Standard Infusion Only Pump 11 Elite) via a tube, is used as the source of droplets, constituted from deionized water. The ejection conditions are so monitored as to ensure zero horizontal velocity of the drop. Considering the falling drop to be spherical, let its radius be r_0, before it impacts against the soap film. It is possible to estimate the order of rotational inertia of the drop by $(2/5)\, m\, {r_0}^2$, which computes out to be approximately 10^{-12} kg m^2, with m being the mass of the drop. Assuming a minimum droplet velocity of about 1 m s^{-1}, the kinetic energy of the falling drop is approximately 10^{-6} J. In order to have rotational energy comparable to the overall kinetic energy, the angular velocity of the drop would have to be about 10^3 rad s^{-1}, which is unrealistic for a setup like ours. Thus, the spin effects can only account for a negligible energy contribution. Flow rate is chosen to ensure that successive droplets are temporally separated in their impact with the film, so as to avoid unwanted wake interactions on the substrate. The needle is mounted on a double axis horizontal-vertical translation stage. Three heights of drop release are selected to achieve three velocities of drop impact. We have 48 bounce-off data-points obtained for these 3 different heights of free descent for the drop, combined with 8 angles of film inclination for each, with 2 trials in each orientation. The imaging protocol includes observing thickness fluctuations (through interferometry) and flow fluctuations (through PIV). For front and side imaging of the impact, we have used digital high speed cameras (Vision Research Phantom v641).

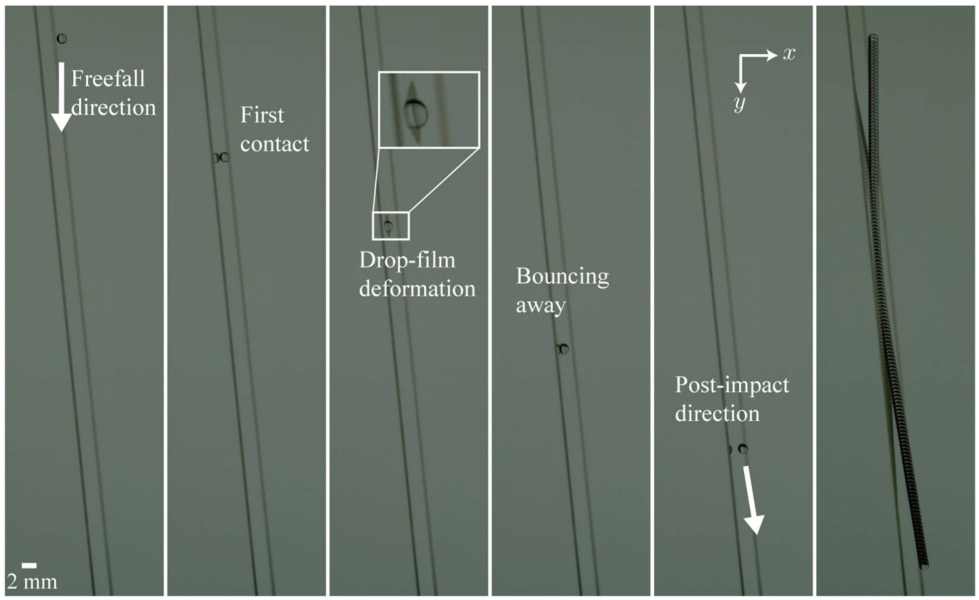

Figure 3. A representative experiment depicting the different stages ((a)–(e)) during the bounce-off regime for a vertically descending droplet impinging on an inclined flowing soap film. Imaging is done with the line of sight being almost in plane with the film, from its lateral side. The different time steps for each of the snapshots are labeled. The droplet deforms the film and is itself maximally deformed about halfway through the contact phase. Panel (c) provides a zoomed-in view of the respective deformations. Panel (f) provides a comprehensive depiction of the impacting drop trajectory, through superposition of images captured at regular time increments. Horizontal direction is represented by the *x*-axis, and *y*-axis marks the vertically downward pre-impact descent direction of the drop. See table 1 for the impact parameters like the pre and post-impact drop speeds, drop size change, and angular orientation of the film.

2.3. Diffused light imaging

The soap film is illuminated normally by a monochromatic sodium light source (with wavelength $\lambda = 532$ nm), the images being recorded at 4500 frames s^{-1} ('front view', refer to figure 2). Additionally, a diffused white light tablet illuminates the film laterally ('side image', refer to figure 2), and the imaging is done by another high speed camera, also at 4500 frames s^{-1}. The diameter of the nylon cables (0.3 mm) is used to determine the length scale of the images. Sodium light interference fringes manifest as contrasting dark and bright regions on the soap film, corresponding to thickness fluctuations, enabling visualization of surface waves and vortices.

Image processing is performed on the collected images in MATLAB (Mathworks Inc., MA, USA) in order to measure the pre-impact drop radius r_0, the spread radius r_s of the drop on impact (in other words, r_s is the radius of the circular peripheral outline formed by the intersection of the impinged portion of the drop with the film plane), and the drop's pre and post-impact velocities v_0 and v_f respectively. Measurement accuracy is constrained by the amount of available contrast between the droplet and its background. For spherical droplets, a circular Hough transform is implemented to measure the radius; but in the deformed drop

case, the droplet height is determined by manually counting the pixels between the edges of the droplet defined by the sharpest gradient of the drop image.

2.4. Particle imaging velocimetry

Hollow glass spheres, of diameter 10 μm, are suspended in the soap solution and a 532 nm continuous wave diode pumped solid state laser at 5–10 W illumination is used to conduct the PIV measurements. The beam is passed through a cylindrical lens to generate a laser sheet, followed by collimation optics to pass the laser sheet from one side of the film to the other. The laser light scattered by the hollow glass tracer particles is captured at 6000 frames s^{-1} (front view, refer to figure 2). This data is post-processed using PIV algorithms written in-house to measure the two-dimensional velocity field through a rectangular grid-based Eulerian approach. Quantitative estimates of the shed vortex momenta use the length-scale measurements of the vortex dipole and its speed with respect to the soap film flow, a technique mentioned by Bush and Hu (2006) while reviewing recent results on biolocomotion on a liquid bath.

3. Reduced parameter model

For a basic physical understanding and to ensure mathematical tractability of the drop-film interaction, we propose a number of idealizations based on the observed experimental features. We assume that the impact does not involve any fluid transfer between the impinging drop and the film substrate. For identifying the parametric region for a specific regime of impact, we conduct a quasistatic analysis of the drop after it has impinged into the film, thereby deforming itself (as the impacting drop spreads out on the film surface) and also the soap film. It is assumed that the kinetic energy from the droplet descent has been used up to deform the film material and the drop undergoes zero transverse-stream motion for an infinitesimal time (in the order of milliseconds, see figure 3)[8]. To gauge the possibility of eventual post-impact bounce-off, we compute the force components acting perpendicular to the film plane, which would aid the drop to bounce. Similar modeling techniques, albeit for different problems of drop impacts have been adopted before, for example by Chappelear (1961), who had studied vertical drop impacts and entrance in a liquid bath. Another simplifying assumption entails that at the point of maximum deformation, the deformed tip of the impacting drop just touches the lower surface of the film substrate. Hence, the depth of the peripheral tip of the impinged volume of the drop from the original plane of the film flow is constrained by the thickness of the film, which also undergoes a peak compressive deformation equal to its thickness at the center of that patch. The resulting deformation contour (figure 4) notably shares similarities with the oblate-ellipsoidal drop deformation often cited in literature (Moláček and Bush 2012). Our experimental design does not allow for an accurate estimation of the film thickness, and hence for the model predictions, we have used published values (1.5 μm; see e.g. Schnipper *et al* (2009)) for comparable setups.

3.1. Force criterion for bounce-off impact

To capture the parameters necessary for the bounce-off regime, the resultant force component perpendicular to the film plane (on the side of the pre-impact drop location) should exceed

[8] The impinged drop propagates downstream with the film flow over the infinitesimal time-window of impact. Velocity gradients between that of the drop along the film plane and the stream flow generate shear layers, which evolve into vortex dipoles.

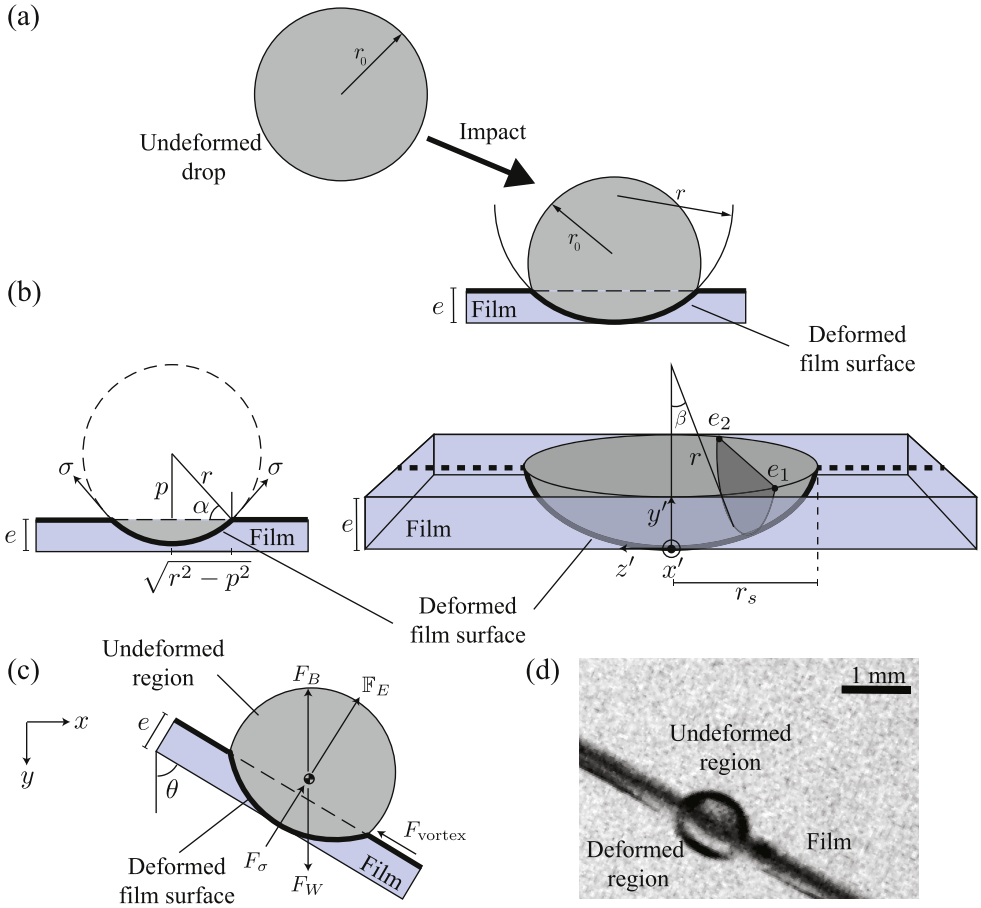

Figure 4. Outlines of the idealized deformed geometries of the drop during its impact on a film of thickness e. See section 3 for the detailed discussion. (a) Schematic view of the drop deformation on impact. Here r_0 is the radius of curvature of the pre-impact undeformed spherical droplet, r is the radius of curvature of the portion of the drop volume that has impinged into the film on impact and has been deformed. (b) Projected view (left) and perspective view (right) of an impinged droplet sliced along the film plane. The latter shows the differential cross-section $e_1 - e_2$ of the deformed film surface used to calculate bulk elastic force on the drop. Here r_s is the radius of the spread outline of the deformed drop intersecting the film plane. A special set of axis is defined here for mathematical expediency in the elastic force calculation. y' is normal to the film plane, x' is transverse to the stream, and z' is directed opposite to the stream flow. (c) Force balance diagram of the quasistatic deformed droplet in contact with the film inclined at angle θ to the vertical. (d) Snapshot of a representative experimental impact. The experiments served as a reference point for the assumed deformation geometry in the model.

zero. This generates the force inequilibrium criterion:

$$\mathbb{F}(r_s, \theta) = F_\sigma(r_s) + \mathbb{F}_E(r_s) + [F_B(r_s) - F_W] \sin\theta > 0, \tag{1}$$

where $\mathbb{F}$ is the resultant force on the impacting drop in the normal direction to the film flow, F_σ is the interfacial tensile force component perpendicular to the stream, $\mathbb{F}_E$ is the bulk elastic force component (assuming linearized elastic deformation transverse to the film flow) normal

to the film surface and flow direction, F_B is the buoyant force, and F_W is the drop weight. See table 2 for a comparison of the orders of magnitude of the different forces acting on a drop as it interacts with the film surface. It is revealed that the elastic force from the film deformation has the least contribution. For a leading order analysis of the drop dynamics, the other possible forces acting on the drop along the film flow plane (like drag forces from the shed vortices, apart from the other streamwise force components from above) are not incorporated in the criterion (i.e. inequality 1).

Figure 4 presents a schematic of the model geometry that facilitates the (r_s, θ) functional reduction of the different force contributions. Spread-out volume of the drop (impinged into the film thereby deforming it as well) is assumed to have r as its radius of curvature (see figure 4(a)). The remaining volume (which is off the film plane) is assumed to maintain its original radius of curvature (r_0). Also, e represents the thickness of the soap film.

Using the above definitions, it can, hence, be shown that

$$r = \frac{{r_s}^2 + e^2}{2e}. \tag{2}$$

For generality, let ρ be the density of the interstitial fluid in the soap film and $\tilde{\rho}$ be the density of the droplet fluid. Note that in our experiments with drops constituted from deionized water and the film solution having a soap concentration of 2.5% by volume, the two densities can be considered to be approximately same and equal to $1000\,\mathrm{kg\,m^{-3}}$. However, similar experiments can also be carried out using a drop made out of a liquid metal in order to drastically change the dependence on liquid densities (e.g. Khoshmanesh *et al* (2017) have used gallium-based liquid metal for microfluidic experiments). With $\mathcal{V}_D$ as the volume of the portion of the drop that has impinged into the film and has deformed, and g being the gravitational acceleration, the buoyant force on the impacting drop, owing to the displaced interstitial fluid, can be expanded as follows:

$$\begin{aligned} F_B &= \rho g \mathcal{V}_D \\ &= \left[\pi \int_p^r (\sqrt{r^2 - p^2})^2 \mathrm{d}p\right]\rho g \\ &= \pi\left[\frac{2}{3}r - (r-e)\left(1 - \frac{(r-e)^2}{3r^2}\right)\right]\rho r^2 g. \end{aligned} \tag{3}$$

Note that in the above, we have utilized $p = r - e$ (see figure 4). Thus, inputting equation (2) in (3), F_B is reducible to a function of r_s. Also, the weight of the impacting drop is simply $F_W = 4\pi\tilde{\rho}g{r_0}^3/3$.

With the model exclusively addressing the bounce-off regime, we only consider the surface tension that is normal to the film plane. Employing the symbols introduced in figure 4, the contribution can be mathematized as

$$\begin{aligned} F_\sigma &= \sigma(2\pi\sqrt{r^2 - p^2})\cos\alpha \\ &= \sigma(2\pi\sqrt{r^2 - (r-e)^2})\frac{\sqrt{r^2 - (r-e)^2}}{r} \\ &= 2\pi\sigma e\left(2 - \frac{e}{r}\right), \end{aligned} \tag{4}$$

where σ is the tensile force per unit length. In our reduced order model, we use previous measurements for soap films, whereby $\sigma = 32.70\ \mathrm{mN\,m^{-1}}$ (Kim and Wu 2010), recorded using a Du Noüy tensiometer; for details on the experimental technique, see e.g.

Lunkenheimer and Wantke (1981). However, to confirm that this value is indeed on the right order of magnitude, we have performed a quasistatic measurement using the well-known pendant drop test (for methods, see e.g. Berry *et al* (2015)). Considering the geometry of a pendant drop of the soapy solution, we measured the radius of curvature at the bottom of the drop, and computed the hanging mass using standard imaging techniques in order to identify the drop edges. From there, assuming equilibrium between surface tension force, gravitational force, Laplace and hydrostatic pressure (Garandet *et al* 1994), we found the surface tension $\sigma = 37.199 \pm 6.962\,\mathrm{mN\,m^{-1}}$; of the same order as in the measurements published by Kim and Wu (2010).

Presence of surfactants (soap molecules) in the film medium generates the so-called Marangoni effect (Couder *et al* 1989). With an increase A in the surface area and resultant thinning in a portion of the film, the surfactant molecules are scattered apart. This leads to an increase in surface tension (σ). Consequently, the restoring force imparts a compressible character to the interstitial fluid. Such elastic effects (Lhuissier and Villermaux 2009) owing to gradients in surface tension is referred to as Marangoni elasticity $E_\mathrm{M} = A(\mathrm{d}\sigma/\mathrm{d}A)$. For the linearized bulk elastic effects of the deformed film material, we just consider the deformation transverse to the film plane, so as to focus on the bounce-off impact. These restitutive forces on the drop are integrated over the entire deformed contour (comprising four symmetrically and transversely compressed quadrants of the interstitial fluid), to obtain

$$\mathbb{F}_\mathrm{E} = 4\,E_\mathrm{M}\int_0^{\cos^{-1}(1-\frac{e}{r})}\int_0^{\mathcal{G}}(e - [\sqrt{r^2 - x^2} + r(2 - \cos\beta)])\mathrm{d}x'\,\mathrm{d}\beta, \qquad (5)$$

where

$$\mathcal{G} = \sqrt{2er(2 - \cos\beta) - r^2(\cos^2\beta - 4\cos\beta + 3) - e^2}.$$

Here the angular parameter β tracks out the spherical annulus of the impinged drop contour from the center of curvature of the impinged volume (see figure 4(b)). Note that since the impact and the resultant deformation occur over a short time scale in a thin substrate; therefore it is contemplated (Couder *et al* 1989) feasible and sufficient to just consider Marangoni elasticity (E_M). Recent measurements by Kim and Mandre (2017) on flowing soap films (through generating an oblique shock in the film and tracking the shock angle and evolution of flow speed and thickness) suggested $E_\mathrm{M} = 22.0\,\mathrm{mN\,m^{-1}}$. This is assumed to stay constant owing to the crowding of the surfactant solution surface with soap molecules, and is the value used in the current results.

3.1.1. Caveat I – role of surface waves. As the drop impacts on the soap film, the interaction generates a free surface wave. The wave speed was approximated to be $2.3\,\mathrm{m\,s^{-1}}$ for the representative example in figure 3, where the soap film was angled at 5.99° to the vertical. Therefore, over the duration of the impact which lasts 0.013 s, counted from panels (b) to (d) in figure 3, the wave front propagates a distance of $230\,\mathrm{cm\,s^{-1}} \times 0.013\ \mathrm{s} = 2.99\,\mathrm{cm}$. It is much less than the distance (5 cm; same as the width of the film) the wave has to cover to return to its point of origin (drop impact zone) after getting rebounded from the hanging wires. With the drop bouncing off before the reflected wave returns, the model justifiably neglects the effects of surface waves on post-impact dynamics of the drop. In some exceptional cases, the wave speed is high enough ($\approx 4.9\,\mathrm{m\,s^{-1}}$ for the film angled at 2.58° to the vertical, as an example) to traverse more than the 5 cm distance during the contact duration of the drop with the film. However, the amount of momentum carried by the wave decays as $1/\mathrm{distance}$ on the (approximately) two-dimensional medium. Therefore, the wave striking the boundary will transfer most of its momentum to the flexible wires and even

though some of it is bounced back to the drop-impact zone, the transmitted momentum contribution will be negligible.

3.1.2. Caveat II – role of trapped air between the drop and the soap film. The drop-impact model discussed here aims to offer a leading order analysis. It does not consider the layer of air posited between the drop and the film as the impact takes place, rather the focus is on gaining a broad physical understanding through the balance of forces acting on the drop. It should, however, be noted that the air layer does matter, especially as the drop approaches the soap film. The film starts to deform before physical contact is made, owing to the air between the drop and the film being squeezed through. If the impact time is longer, the intermediate air layer can drain out to a critical thickness across which intermolecular van der Waals forces would promote coalescence. Marrucci (1969) presents a related study on the coalescence of two in-contact bubbles. See also Meleán and Sigalotti (2005) for a numerical study on the coalescence of liquid drops, effected by van der Waals forces. Nuances as those are, however, not covered in the discussed reduced parameter model.

3.1.3. Caveat III – on the thickness of the flowing soap film. In our experiments, the surface wave speeds (v_s, let) vary over a range of approximately 2–7 m s^{-1}. Consequently, it can be shown that the the range of film thickness (e) varies from around 1.3 to 16.3 μm, via $e = 2\sigma/(\rho\, v_s^2)$ (Couder *et al* 1989). Films with such interstitial dimensions can be considered 'thick films', and as such, they behave as Newtonian fluids, with the dynamics governed by the general hydrodynamic principles. We assume that owing to air drag, a terminal velocity is attained in the film, and hence the drop impact zone (film test section) displays uniform free-stream velocity profile along with constant thickness, which we assume to be 1.5 μm, as measured in a similar setup by Schnipper *et al* (2009). The gravity-driven film flow is maintained by a constant pressure head (through re-circulatory pumping). A more rigorous analysis on characterizing the role of film thickness on impacting drop dynamics, while beyond the scope of this work, can however be of significant interest for a future study.

3.2. Phase space representation

Replacing r with the function of r_s (as per equation (2)), the obtained force terms can be exported to inequality 1 to evaluate $\mathbb{F}(r_s, \theta)$. Subsequently, the two extremal contour values of $\mathbb{F}(r_s, \theta)$ occur for $\sin\theta = \pm 1$. The parameters for the bounce-off case should, hence, be inside the (r_s, θ) region bounded by these extremal contours, and in the phase portrait, we focus on the angular range $\theta \in [0°, 90°]$ to secure a film orientation compatible with the experimental setup. Figure 5 locates the experimental data points on the $(r_s/r_0, \theta)$ plane. Solid gray contour lines are for the extremal cases of $\mathbb{F}(r_s, \theta)$ for choice of $r_0 = 0.691$ mm. Dashed gray contour lines represent the extremal cases of $\mathbb{F}(r_s, \theta)$ for choice of $r_0 = 0.6$ mm. Thus, angular inclination of the soap film and the non-dimensional spreading parameter of the drop chart out the phase space domain and the physical parametric bounds that characterize the post-impact drop behavior. The ratio r_s/r_0 quantifies the dimensionless spreading of the drop as it impinges into the film surface.

For phase sub-region II, the higher angles of inclination lead to sagging of the film, which can induce incoming contaminating flows from the peripheries on to the test section. Such complexities are beyond the scope of our modeling framework. Further, with higher angles of attack, the momentum transfer of the drop to the film transverse to its plane of flow is high enough. The film initially *withstands* the transferred momentum allowing the drop to 'coalesce' with the stream. But, with increasing momenta transfer normal to the film, it

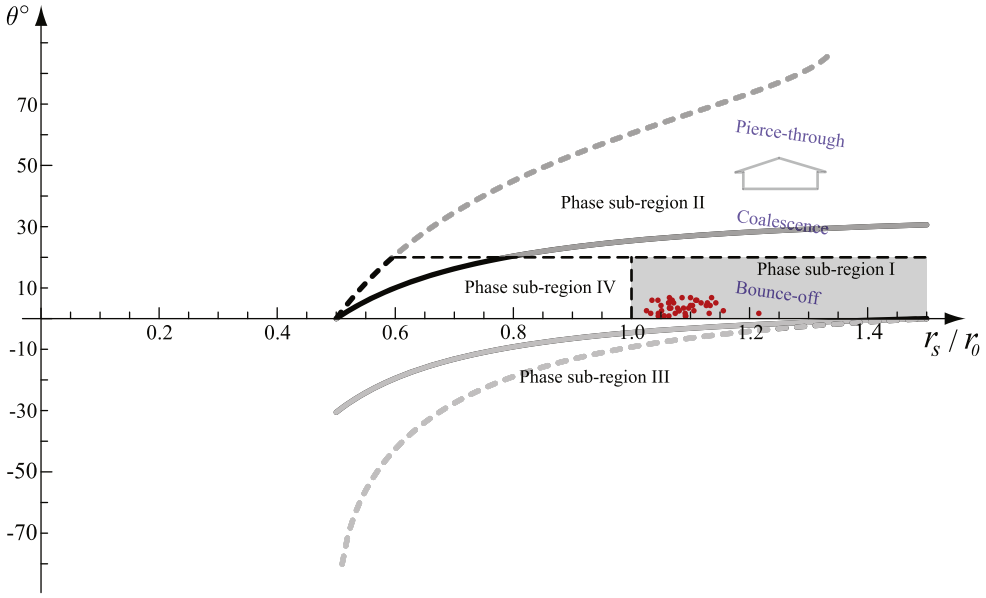

Figure 5. Phase space representation for the bounce-off regime. Vertical axis represents the angle (θ, in degrees) between the pre-impact drop trajectory and the inclined flowing soap film. Horizontal axis characterizes the spreading trends of the drop as it hits the film, in terms of the ratio between its post and pre-impact dimensions (r_s/r_0). The small solid circles indicate the phase space positions of the 48 experimental data-points recorded. For the input parameter, we use the observed global mean (0.691 mm) as well as a lower estimate (0.6 mm, to account for observational inaccuracies) for the experimental pre-impact drop radii (r_0). The solid demarcating lines correspond to the observed mean, while the dashed demarcating lines come from assuming the lower estimate. These lines delineate the model region in the phase space, that would correspond to a bounce-off regime. The horizontal axis quantifies the spread of the drop as it hits the film surface. Phase sub-region I (colored gray) marks the parametric space that theoretically corresponds to the bounce-off regime. All the data-points lie in the predicted model region (intersection of the regions predicted using the two extremal estimates of r_0). The sub-regions II (with higher angles of inclination, sagging becomes appreciable; also this parametric region is gradually marked by the emergence of coalescence and piercing regimes), III (where $r_s < r_0$, thus defying the experimental visualizations), and IV (corresponds to negative film inclination angles) comprise physically untenable parameters for a bounce-off impact. The slanted labels mark the approximate regions of the different impact regimes. We have used Marangoni elasticity modulus $E_M = 22.0 \times 10^{-3}$ N m^{-1} (see Kim and Mandre (2017)) and surface tension coefficient $\sigma = 32.7 \times 10^{-3}$ N m^{-1} (see Kim and Wu (2010)). Section 3 discusses the related details.

gradually starts to thin out in a patch; eventually permitting the drop to tunnel through the film (without actually rupturing the film). This, we identify as the 'pierce-through' regime. We consistently observed such pierce-through dynamics for a number of trial experiments we had conducted with θ ranging from 60° to 90°. In phase sub-region III, the dispersion condition $r_s < r_0$ defies the experimental observation that the small drops mostly spread out on impact. Finally, phase sub-region IV consists of negative angles of inclination and is merely a *mathematical abstraction* owing to the dependence of $\mathbb{F}$ on θ, since the phase space contour limits in figure 5 are based on the trigonometric restriction $\sin\theta \in [-1, 1]$.

Phase sub-region I (colored gray in figure 5) represents the predicted model parameter space for the observed bounce-off regime. Its vertical extent is marked by the dashed line at 20° inclination. However, it is an open question as to at what angle the film sagging becomes appreciable (which consequently results in contamination of the impact region from peripheral flows) and this demarcation is just a very conservative estimate. The horizontal extent of the region is determined based on the observation that the drop always deforms and spreads out (i.e. $r_s > r_0$). Comparison with experiments turns out satisfactory as all the experimental data-points could be located in the predicted phase domain.

4. Momentum transfer and natural world analogs

A quasistatic transverse-stream projection of the bounce-off regime resembles (see figures 6(a) and (b)), at least qualitatively, the impulsive interaction observed in water strider locomotion at air–water interfaces. It is, however, crucial to note that the two are widely disparate systems, with the most significant differences being the infinite depth consideration for the liquid bath in case of insect locomotion analysis, and the fact that soap films have thicknesses in the order of microns along with a confined lateral extent (stretching between the hanging wires). Figure 6(a), adapted with permission from Hu *et al* (2003), depicts a schematic of the interfacial interaction when a water-strider jumps off the air–water interface. Like the insect, the drop acts like a bluff body on the interface and generates waves and vortices owing to the relative motion with respect to the background soap film stream. To explore the dynamical connection between these two unrelated interactions, we refer to the theory on impulsive fluid forcing of water walking animals, proposed by Bühler (2007). The analysis assumes a quiescent liquid bath of infinite depth and looks at the interaction at its interface. The insect pushes against the water surface transferring momentum to the bath, and it itself jumps off the surface owing to the impulsive reaction. For the horizontal momentum transferred to the bath, $1/3$ of it is taken up by the generated free surface waves, and $2/3$ is accounted for by the shed vortices. We apply the same theory in the current system to ascertain the momentum carried by the shed vortex dipole (see figure 7), as per Bühler (2007). The pre-impact and post-impact velocities of the drop, as measured from the experiments reveal that the drop gains in momentum as it bounces off. We assume that an impulsive momentum of equal magnitude is transmitted to the film. Subsequently, $2/3$ of the imparted momentum along the film plane is calculated to theorize the momenta ($\mathbb{P}_{\mathrm{VD_B}}$) purportedly carried by the shed vortex dipole, as hereunder:

$$\mathbb{P}_{\mathrm{VD_B}} = \frac{2m}{3}(v_{f_y}\cos\theta + v_{f_x}\sin\theta - v_{0_y}\cos\theta), \tag{6}$$

where m is the mass of the drop, v_{0_y} is the measured vertically downward component of the pre-impact drop velocity (the horizontal component is monitored to be approximately zero), and v_{f_x}, v_{f_y} are respectively the measured horizontal and vertical components of the post-impact drop velocity, just after it has disconnected itself from the film surface. The mean order of the dipole momenta values comes out as 10^{-7} N s.

The estimates from Bühler's theory are compared to the dipole momenta calculated from PIV data, through extracting the positional evolution of the coherent vortex structures. These latter values of course provide more accurate quantification for the mometum transfer during the impact. Based on these measurements, the mean momentum carried by the shed vortex dipole is 7.425×10^{-7} N s. As a caveat, it should be however noted that this estimate leaves out the data-points for the largest impact angle that approaches break-down of the model

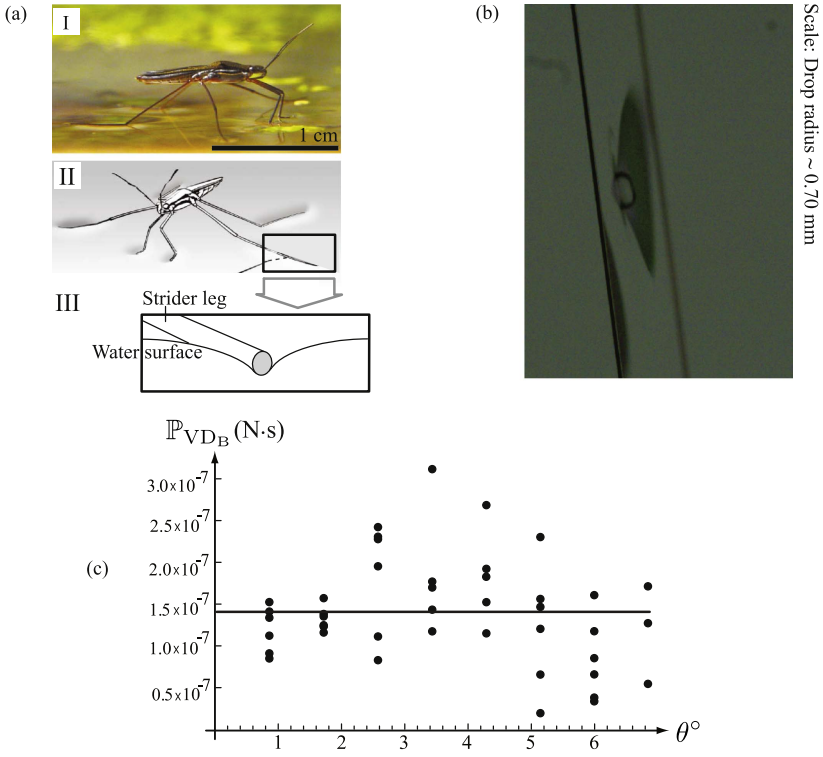

Figure 6. (a) Panels I–III in (a) have been reprinted by permission from Macmillan Publishers Ltd: Nature [Hu *et al* (2003)], Copyright (2003). Panel I shows a natural water strider (*Gerris remigis*) at the air–water interface. Panels II and III present a cartoon of the interfacial distortion when the strider sits static at the air–water interface, but is about to 'jump'. (b) A representative bounce-off regime as observed in our drop-film impact experiments. The drop deforms and spreads out, as it impinges in and deforms the soap film. (c) Experimental dipole momenta computed from Bühler's theory (see Bühler (2007)), using the observed mean pre-impact drop radius of 0.691 mm. The average momentum comes out as 1.421×10^{-7} N s (shown by the black horizontal line). Momenta values retain the same order even if we consider the lower estimate for r_0, which is 0.60 mm. The averaged vortex dipole momenta then comes out as 0.930×10^{-7} N s. The pre and post-impact velocities of the drop are used to measure the momentum transfer to the film during this impulse action, subsequently from which the momenta proportions, shared between the shed vortices and the capillary waves, are computed. θ (in degrees) on the horizontal axis marks the experimental angles subtended by the soap film and the pre-impact drop trajectory. Along the vertical axis, we plot $\mathbb{P}_{VD_B}$ which represents the shed vortex dipole momenta in the experimental impacts, computed according to Bühler's theory.

idealization (for example, the idealization does not consider any sagging). If we include those numbers, the mean dipole momentum shoots up to 18.191×10^{-7} N s. So, while the order overall matches with the global mean estimate (1.252×10^{-7} N s, averaged from table 3) using Bühler's analysis; the experimental dipole momentum is still higher. The reasons can be attributed to the following:

- Soap film, owing to being stretched taut over the wired network in the experimental setup, manifests a distinct trampoline effect, as excellently discussed by Gilet and Bush (2009b)

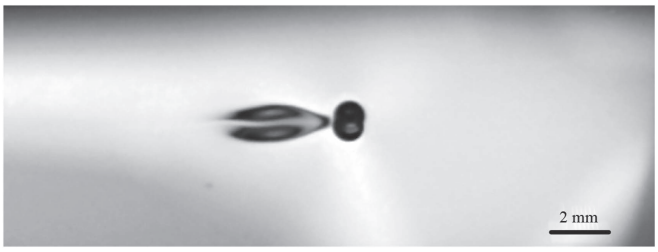

Figure 7. The drop acts like a bluff body on the film flow during the duration of impact (owing to the relative velocities between the two) and sheds a vortex dipole (along with the generation of capillary waves). Air layers trapped between the drop and the film try to squeeze out, thus transmitting viscous stresses to the film. These stresses induce the formation of shear layers, which eventually evolve into vortex dipoles. The above image is captured using a monochromatic sodium lamp as the source of light. Note that the monochromatic light source casts a shadow of the drop on the film surface, as the drop bounces away. The thickness fluctuations assist in determining the vortex cores. PIV data for similar experiments (using planar laser beam as the light source; method described in section 2.4) give us the flow velocity field and the accurate dipole momenta can be calculated by tracking the dynamic vortex cores.

in their seminal work. This provides an additional push on the bouncing drop thereby increasing the recoil momentum.

- Bulk elastic deformation of the film results in additional restitutive forces. This effect is absent in static liquid baths of infinite depth, a key assumption by Bühler (2007).

5. Conclusions

To summarize, this study delineates the experimental parameters for bounce-off impact of drops (1.2–1.4 mm diameter; constituted from deionized water) after obliquely striking an inclined flowing soap film (made from 2.5% soap solution). Figure 1 provides a cartoon of the various impact types, while figure 2 contains a sketch of the experimental setup. Representative experimental visuals are shown in figure 3 (see table 1 for the relevant parameters). Section 2 charts out the experimental methods.

As a means to identify the experimental parameter space that prompts the bounce-off regime, we have proposed a reduced parameter model (see section 3). In the modeling framework (see figure 4 for the model schematics), the angular inclination of the soap film and the on-impact deformation features of the drop quantified by the ratio of its post-impact (spread out) and pre-impact radii constitute the phase plane parameters. The predicted model phase space fits well with the broad population of experimental observations. Figure 5 demonstrates the corresponding phase portrait, with the model phase zone for bounce-off drop impact labeled as phase sub-region I. All the experimental data-points belong to this predicted model zone. Our interests in the problem trace back to the scarcity of interactions which evidence in-tandem roles of bulk elasticity and hydrodynamics in a fluidic system, as have been seen here. The reduced order model was designed to explore the effects of bulk elasticity of the deformable film material on the dynamics of impacting drops. However, the results confirm that the elastic force indeed has the smallest contribution towards effecting the drop bounce-off. See table 2 for an order-of-magnitude comparison of the contributive force components.

Table 1. Parameters for the representative drop-film interaction portrayed in figure 3. Symbols: $v_{0_x} \equiv$ horizontal component of the pre-impact drop velocity, $v_{0_y} \equiv$ vertical component of the pre-impact drop velocity, $v_{f_x} \equiv$ horizontal component of the post-impact drop velocity, $v_{f_y} \equiv$ vertical component of the post-impact drop velocity, and θ is the inclination angle of the flowing soap film to the vertical. For the x and y directions, see figures 3 and 4.

Parameters	Physical estimates
r_0	0.6844 mm
r_s/r_0	1.0669
v_{0_x}	0 mm s^{-1}
v_{0_y}	1009.03 mm s^{-1}
v_{f_x}	168.14 mm s^{-1}
v_{f_y}	1075.27 mm s^{-1}
θ	5.99°

Table 2. Comparison of the orders of magnitude of different forces acting on the impacting drop. We list the force estimates for two selections of the pre-impact drop sizes: $r_0 = 0.691$ mm (global mean pre-impact drop radius) and $r_0 = 0.6$ mm.

Forces	$r_0 = 0.691$ mm	$r_0 = 0.6$ mm
F_σ	$4.109\,30 \times 10^{-1}$ N	$4.109\,10 \times 10^{-1}$ N
$\mathbb{F}_E$	$1.555\,08 \times 10^{-13}$ N	$1.555\,08 \times 10^{-13}$ N
F_B	$2.756\,36 \times 10^{-9}$ N	$2.078\,18 \times 10^{-9}$ N
F_W	$13.54\,41 \times 10^{-6}$ N	$8.866\,83 \times 10^{-6}$ N

Table 3. Shed vortex dipole momenta ($\mathbb{P}_{VD_B}$) for some typical pre-impact drop sizes. The values have been derived based on Bühler's theory (see Bühler (2007)) using the measured pre and post-impact drop velocities.

Pre-impact drop radius r_0	$\mathbb{P}_{VD_B}$
0.60 mm	0.9303×10^{-7} N s
0.65 mm	1.1828×10^{-7} N s
0.691 mm	1.4210×10^{-7} N s
0.70 mm	1.4733×10^{-7} N s

As a final interesting observation, the drop-film impact demonstrates remarkable qualitative similarity (figure 6) to the interfacial dynamics observed at the air–water boundary during the impulsive locomotion of water-walking insects, with perhaps the most significant distinguishing feature between the two phenomena being the varying roles of system elasticity, in lieu of the recoil momentum exerted by the infinite-depth fluid bath and the microns-thick soap film on the insect and on the drop, respectively. However, quite strikingly the vortex dipole momenta imparted to the fluid substrate reveal the same order (10^{-7} N s) in both the systems. This unexpected congruity suggests that this impulsive bounce-off regime for drops impinging on soap films may be explored as a simple analog for the impulse-based locomotion of many aquatic insects at the air–water interface.

Acknowledgments

SB, AY, and MB were supported by the Collective Interactions Unit, OIST Graduate University. Additionally, AC was partially supported by Fondecyt 11130075.

ORCID iDs

Saikat Basu https://orcid.org/0000-0003-1464-8425

References

Bandi M, Concha A, Wood R and Mahadevan L 2013 A pendulum in a flowing soap film *Phys. Fluids* **25** 041702
Basu S 2014 Dynamics of vortices in complex wakes: modeling, analysis, and experiments *PhD Thesis* Virginia Polytechnic Institute and State University
Basu S and Stremler M A 2017 Exploring the dynamics of '2P' wakes with reflective symmetry using point vortices *J. Fluid. Mech.* **831** 72–100
Basu S, Yawar A, Concha A and Bandi M 2015 Modeling drop impacts on inclined flowing soap films *Bull. Am. Phys. Soc.* **60** 211
Berry J D, Neeson M J, Dagastine R R, Chan D Y and Tabor R F 2015 Measurement of surface and interfacial tension using pendant drop tensiometry *J. Colloid Interface Sci.* **454** 226–37
Bühler O 2007 Impulsive fluid forcing and water strider locomotion *J. Fluid Mech.* **573** 211–36
Bush J W and Hu D L 2006 Walking on water: biolocomotion at the interface *Annu. Rev. Fluid Mech.* **38** 339–69
Chappelear D 1961 Models of a liquid drop approaching an interface *J. Colloid Sci.* **16** 186–90
Chen X, Mandre S and Feng J J 2006 Partial coalescence between a drop and a liquid–liquid interface *Phys. Fluids* **18** 051705
Cheng L 1985 Biology of halobates (heteroptera: Gerridae) *Annu. Rev. Entomol.* **30** 111–35
Couder Y, Chomaz J and Rabaud M 1989 On the hydrodynamics of soap films *Physica* D **37** 384–405
Courbin L, Marchand A, Vaziri A, Ajdari A and Stone H A 2006 Impact dynamics for elastic membranes *Phys. Rev. Lett.* **97** 244301
Courbin L and Stone H A 2006 Impact, puncturing, and the self-healing of soap films *Phys. Fluids* **18** 091105
Garandet J P, Vinet B and Gros P 1994 Considerations on the pendant drop method: a new look at tate's law and harkins' correction factor *J. Colloid Interface Sci.* **165** 351–4
Gharib M and Derango P 1989 A liquid film (soap film) tunnel to study two-dimensional laminar and turbulent shear flows *Physica* D **37** 406–16
Gilet T and Bush J W 2009a Chaotic bouncing of a droplet on a soap film *Phys. Rev. Lett.* **102** 014501
Gilet T and Bush J W 2009b The fluid trampoline: droplets bouncing on a soap film *J. Fluid Mech.* **625** 167–203
Gilet T and Bush J W 2012 Droplets bouncing on a wet, inclined surface *Phys. Fluids* **24** 122103
Gilet T, Vandewalle N and Dorbolo S 2007 Controlling the partial coalescence of a droplet on a vertically vibrated bath *Phys. Rev.* E **76** 035302
Gopinath A and Koch D L 2001 Dynamics of droplet rebound from a weakly deformable gas–liquid interface *Phys. Fluids* **13** 3526–32
Honey E and Kavehpour H 2006 Astonishing life of a coalescing drop on a free surface *Phys. Rev.* E **73** 027301
Hu D L, Chan B and Bush J W 2003 The hydrodynamics of water strider locomotion *Nature* **424** 663–6
Jayaratne O and Mason B 1964 The coalescence and bouncing of water drops at an air/water interface *Proc. of the Royal Society of London A: Mathematical, Physical and Engineering Sciences* vol 280 (The Royal Society) pp 545–65 (http://rspa.royalsocietypublishing.org/content/280/1383/545)
Khoshmanesh K, Tang S-Y, Zhu J Y, Schaefer S, Mitchell A, Kalantar-Zadeh K and Dickey M D 2017 Liquid metal enabled microfluidics *Lab Chip* **17** 974–93
Kim I and Mandre S 2017 Marangoni elasticity of flowing soap films *Phys. Rev. Fluids* **2** 082001
Kim I and Wu X 2010 Tunneling of micron-sized droplets through soap films *Phys. Rev.* E **82** 026313

Kirstetter G, Raufaste C and Celestini F 2012 Jet impact on a soap film *Phys. Rev.* E **86** 036303
Le Goff A, Courbin L, Stone H and Quéré D 2008 Energy absorption in a bamboo foam *Europhys. Lett.* **84** 36001
Lhuissier H and Villermaux E 2009 Destabilization of flapping sheets: the surprising analogue of soap films *C. R. Mec.* **337** 469–80
Lunkenheimer K and Wantke K-D 1981 Determination of the surface tension of surfactant solutions applying the method of lecomte du noüy (ring tensiometer) *Colloid Polym. Sci.* **259** 354–66
Lyklema J and Mysels K J 1965 A study of double layer repulsion and van der waals attraction in soap films *J. Am. Chem. Soc.* **87** 2539–46
Marrucci G 1969 A theory of coalescence *Chem. Eng. Sci.* **24** 975–85
Meleán Y and Sigalotti L D G 2005 Coalescence of colliding van der waals liquid drops *Int. J. Heat Mass Transfer* **48** 4041–61
Moláček J and Bush J W 2012 A quasi-static model of drop impact *Phys. Fluids* **24** 127103
Okumura K, Chevy F, Richard D, Quéré D and Clanet C 2003 Water spring: a model for bouncing drops *Europhys. Lett.* **62** 237
Pan K L and Law C K 2007 Dynamics of droplet–film collision *J. Fluid Mech.* **587** 1–22
Rutgers M, Wu X and Daniel W 2001 Conducting fluid dynamics experiments with vertically falling soap films *Rev. Sci. Instrum.* **72** 3025–37
Salkin L, Schmit A, Panizza P and Courbin L 2016 Generating soap bubbles by blowing on soap films *Phys. Rev. Lett.* **116** 077801
Schnipper T, Andersen A and Bohr T 2009 Vortex wakes of a flapping foil *J. Fluid Mech.* **633** 411–23
Stremler M A and Basu S 2014 On point vortex models of exotic bluff body wakes *Fluid Dyn. Res.* **46** 061410
Stremler M A, Salmanzadeh A, Basu S and Williamson C H 2011 A mathematical model of 2P and 2C vortex wakes *J. Fluids Struct.* **27** 774–83
Terwagne D, Ludewig F, Vandewalle N and Dorbolo S 2013 The role of the droplet deformations in the bouncing droplet dynamics *Phys. Fluids* **25** 122101
Thoroddsen S and Takehara K 2000 The coalescence cascade of a drop *Phys. Fluids* **12** 1265–7
Yawar A, Basu S, Concha A and Bandi M 2015 Experimental study of drop impacts on soap films *Bull. Am. Phys. Soc.* **60** 211